Boutelier, D., Oncken, O., Cruden, A. (2012): Fore-arc deformation at the transition between collision and subduction: insights from 3D thermo-mechanical laboratory experiments. - Tectonics, 31, TC2015

DOI: 10.1029/2011TC003060

Fore-arc deformation at the transition between collision and subduction: Insights from 3-D thermomechanical laboratory experiments

D. Boutelier,[1] O. Oncken,[2] and A. Cruden[1]

Received 2 November 2011; revised 23 January 2012; accepted 26 February 2012; published 24 April 2012.

[1] Three-dimensional thermomechanical laboratory experiments of arc-continent collision investigate the deformation of the fore arc at the transition between collision and subduction. The deformation of the plates in the collision area propagates into the subduction-collision transition zone via along-strike coupling of the neighboring segments of the plate boundary. In our experiments, the largest along-strike gradient of trench-perpendicular compression does not produce sufficiently localized shear strain in the transition zone to form a strike-slip system because of the fast propagation of arc lithosphere failure. Deformation is continuous along-strike, but the deformation mechanism is three-dimensional. Progressive along-strike structural variations arise because coupling between neighboring segments induces either advanced or delayed failure of the arc lithosphere and passive margin. The modeling results suggest that orogenic belts should experience deeper subduction of continental crust and hence higher-pressure metamorphism where the two plates first collided than elsewhere along the plate boundary where collision subsequently propagated. Furthermore, during the initial stage of collision the accretionary wedge is partially subducted, which leads to lubrication of the interplate zone and a reduction of shear traction. Therefore, a large convergence obliquity angle does not produce a migrating fore-arc sliver. Rather, the pressure force generated by subduction of the buoyant continental crust causes fore-arc motion. It follows that convergence obliquity during collision does not yield trench-parallel deformation of the fore arc and its influence on the collision process is limited. However, convergence obliquity may control the geometry of the active margin during the oceanic subduction stage prior to collision, and inherited structures may influence the propagation mechanism.

Citation: Boutelier, D., O. Oncken, and A. Cruden (2012), Fore-arc deformation at the transition between collision and subduction: Insights from 3-D thermomechanical laboratory experiments, *Tectonics*, *31*, TC2015, doi:10.1029/2011TC003060.

1. Introduction

[2] Collisions between continents and volcanic island arcs are common elements in the ancient to recent tectonic history of the Earth. Many of these collisions are oblique and diachronous, starting where the two plates first collide then closing gradually like a zipper. This implies that at any time during an arc-continent collision, some parts record advanced evolutionary stages with the rise of high mountains, whereas in others areas the collision is still to take place. This concept, known as the space-for-time substitution hypothesis, has been used by geologists to understand the process of collision because, ideally, all steps in its temporal evolution are exposed simultaneously and can therefore be investigated by traveling along the length of the plate boundary [*Suppe*, 1984]. The hypothesis has also motivated geodynamic modelers to carry out two-dimensional analog and numerical experiments to investigate the mechanics of arc-continent collision [*Davis et al.*, 1983; *Chemenda et al.*, 1997; *Kaus et al.*, 2008; *Yamato et al.*, 2009; *Dymkova et al.*, 2010; *Afonso and Zlotnik*, 2011]. Although the space-for-time substitution is a powerful and accepted tool in tectonic analysis, it relies on the fundamental and unproven assumption that ongoing deformation in one segment of a plate boundary is mechanically independent from ongoing deformation and deformation history elsewhere along that boundary and that, at the same time, deformation is continuous along the strike of the plate boundary. Geological and geophysical observations in Taiwan, Timor, and Papua New Guinea [*Abers and McCaffrey*, 1994; *Malavieille et al.*, 2002; *Wallace et al.*, 2004; *Nugroho et al.*, 2009] question the validity of this assumption, as they

[1]School of Geosciences, Monash University, Clayton, Victoria, Australia.
[2]Helmholtz Centre Potsdam, GFZ German Research Centre for Geosciences, Telegrafenberg, Potsdam, Germany.

0278-7407/12/2011TC003060

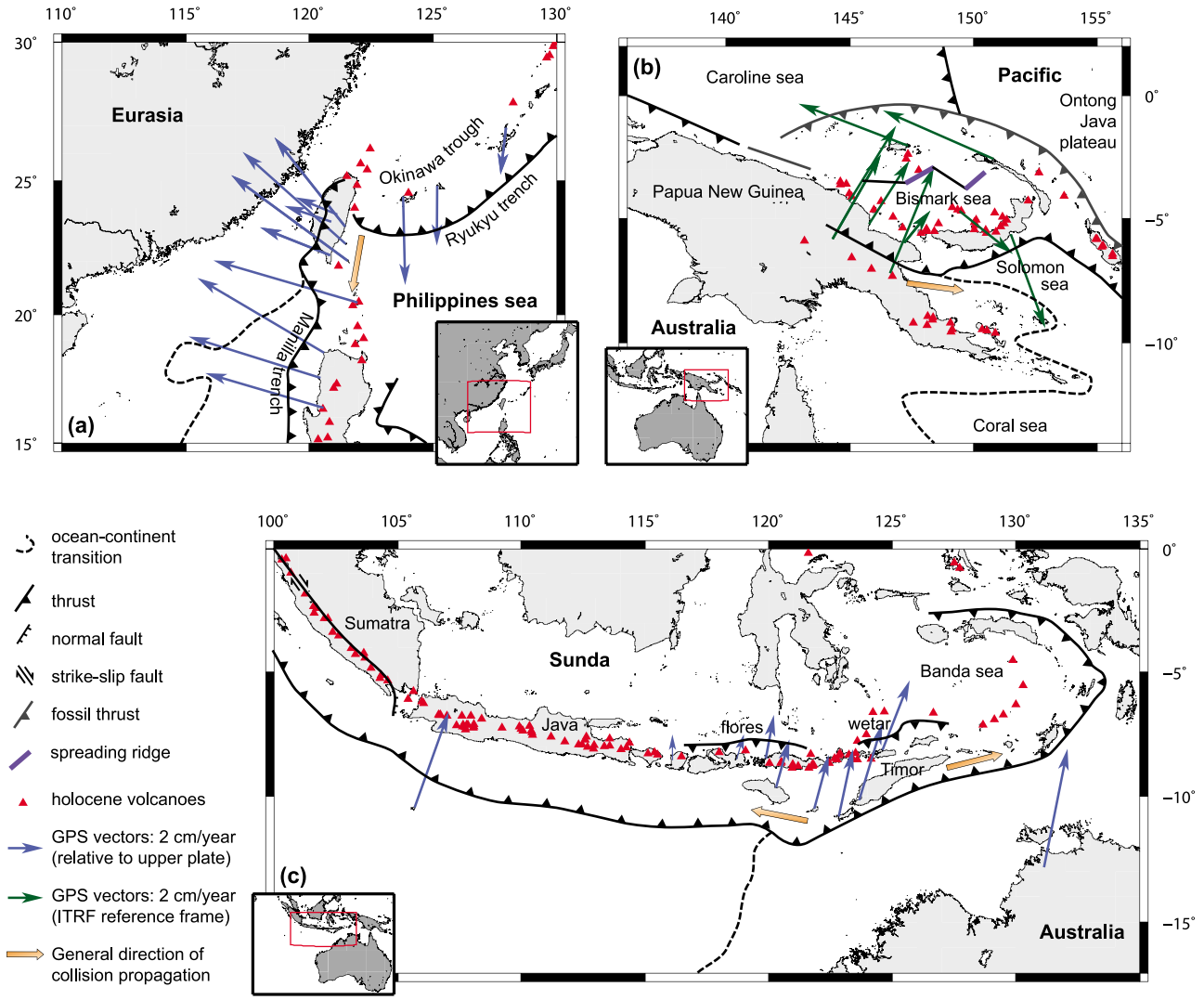

Figure 1. Geodynamic maps of (a) Taiwan, (b) Papua New Guinea, and (c) Timor where arc-continent collisions propagate along the plate boundary. GPS vectors for Taiwan, Ryukyu, and Philippines [*Yu et al.*, 1997; *Nakamura*, 2004; *Yu et al.*, 2012], GPS vectors for Timor [*Nugroho et al.*, 2009], and GPS vectors for Papua New Guinea [*Wallace et al.*, 2004]. Holocene volcanoes [*Siebert and Simkin*, 2002].

suggest that the older and more advanced stages of collision influence how the propagating collision develops (Figure 1), and that major along-strike deformation discontinuity may occur in the form of strike-slip systems segmenting the orogen [*Malavieille et al.*, 2002]. This new interpretation suggests that the four-dimensional thermomechanical evolution (i.e., in space and time) of arc-continent collisions is more complex than usually considered.

[3] Using a new three-dimensional thermomechanical analog modeling apparatus [*Boutelier and Oncken*, 2011], we investigate how an arc-continent collision propagates laterally and how neighboring segments of the plate boundary influence each other. We hypothesize that along-strike gradients in arc-perpendicular normal compression that arise due to the geometry of the passive margin or obliquity of convergence in the trench can lead to trench-perpendicular shearing of the fore arc, which would invalidate the space for time substitution hypothesis as well as the use of 2-D models. We investigate whether there is threshold obliquity above which the shear strain gradient is large enough to create a strike-slip system through the fore arc and thus a major discontinuity in the propagation of the collision. We then investigate the effect of convergence obliquity and hypothesize that trench-parallel horizontal displacement of a fore-arc sliver may also generate a major discontinuity in the propagation of the collision.

2. Oblique Subduction and Oblique Passive Margin

[4] An arc-continent collision can be diachronous because of the obliquity angles ϕ and θ between the convergence vector and the strike of the passive and active margins, respectively (Figure 2). We first consider the effect of the passive margin obliquity angle ϕ (Figures 2a and 2b). If the convergence vector is perpendicular to the strike of the trench, but not to the strike of the passive margin, collision initiates in one location and then propagates laterally

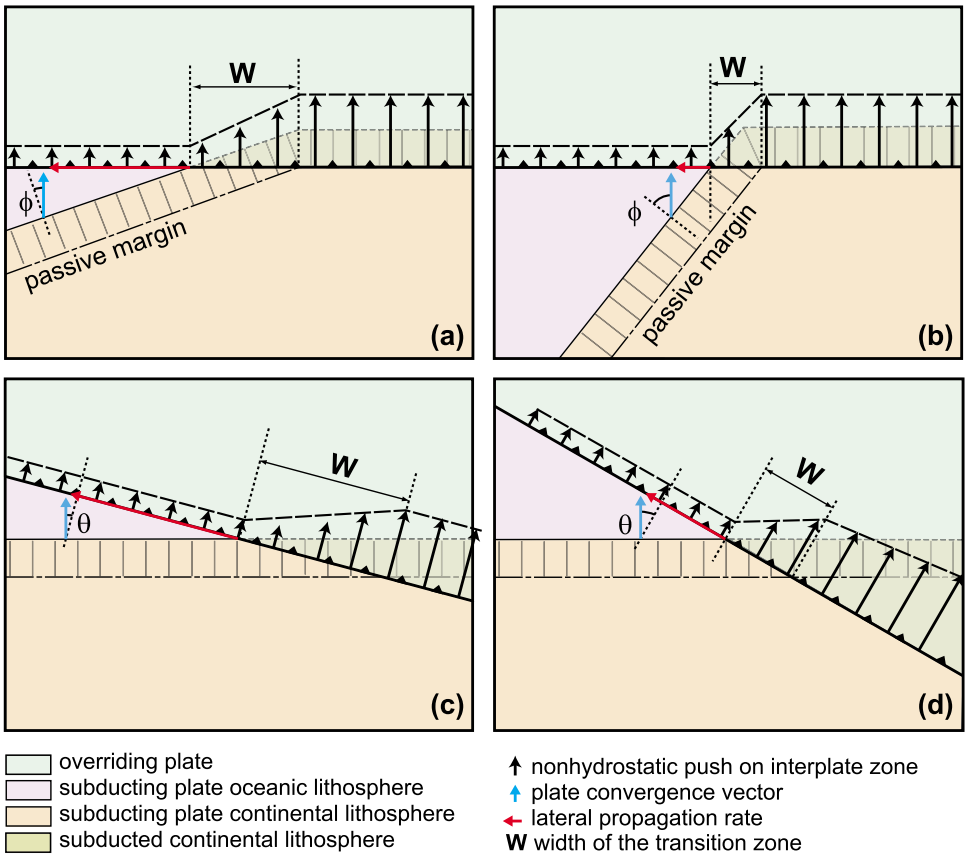

Figure 2. Sketches of the evolution of the width of the transition zone between collision and subduction with the obliquity angles of the passive and active margins, ϕ and θ, respectively. (a) Small and (b) large obliquity angle of the passive margin. Along-strike gradient of compression increases with decreasing width of the transition zone and thus increases with obliquity angle ϕ of the passive margin. (c) Small and (d) large obliquity angle of the active margin. The width of the transition zone decreases with increasing obliquity angle θ of the passive margin.

(Figures 2a and 2b). Consequently, along the strike of the trench there is a gradient in the amount of subducted continental crust. If the passive margin is approximately linear then we can assume that this gradient is also approximately linear. Because of its buoyancy, the subducted continental crust exerts a nonhydrostatic normal stress on the plate boundary whose depth-averaged value increases with the quantity of subducted crust [*Chemenda et al.*, 1995, 1996]. Therefore, the trench-parallel gradient in the amount of subducted continental crust must produce a gradient of nonhydrostatic normal stress due to its buoyancy (Figures 2a and 2b). The magnitude of this gradient increases with increasing obliquity angle, as the width of the transition zone between subduction and collision decreases (Figures 2a and 2b). We hypothesize that this gradient could lead to shearing of the fore arc via the formation of a fault with a significant component of horizontal slip through the fore arc [*Malavieille et al.*, 2002]. However, such a fault may not develop when the gradient is low. Therefore, there may be a threshold obliquity angle above which the gradient of nonhydrostatic stress induces convergence-parallel shear of the fore arc. In such cases, deformation will not be continuous along the strike of the orogen.

[5] A gradient in nonhydrostatic normal stress on the plate boundary may also arise because of the obliquity of subduction in the trench. The angle θ between the convergence vector and the normal to the strike of the trench defines the subduction obliquity angle (Figures 2c and 2d). With larger subduction obliquity angles, the width of the transition zone decreases and therefore the magnitude of the trench-parallel gradient of nonhydrostatic normal stress increases (Figures 2c and 2d). Furthermore, the effects of both obliquity angles, ϕ and θ, on the gradient of nonhydrostatic normal stress may add up or subtract, depending on their orientation. For example in Taiwan the convergence vector is oriented NW–SE, the trench is approximately NNE–SSE, and the passive margin is roughly NE–SW (Figure 1a). Therefore, ϕ is positive (in the trigonometric sense) while θ is negative and their respective effects add up. Consequently, the collision propagates slowly to the south and a large gradient in nonhydrostatic normal stress is expected.

[6] There is, however, a fundamental difference between lateral propagation due to the obliquity of subduction and lateral propagation due to the obliquity of the passive margin. In the first case, the upper plate is subjected to an oblique shear traction in which the horizontal trench-parallel component drags the fore arc along the trench [*Fitch*, 1972; *Chemenda et al.*, 2000b]. In turn, the trench-parallel motion of a fore-arc sliver toward or away from the collision

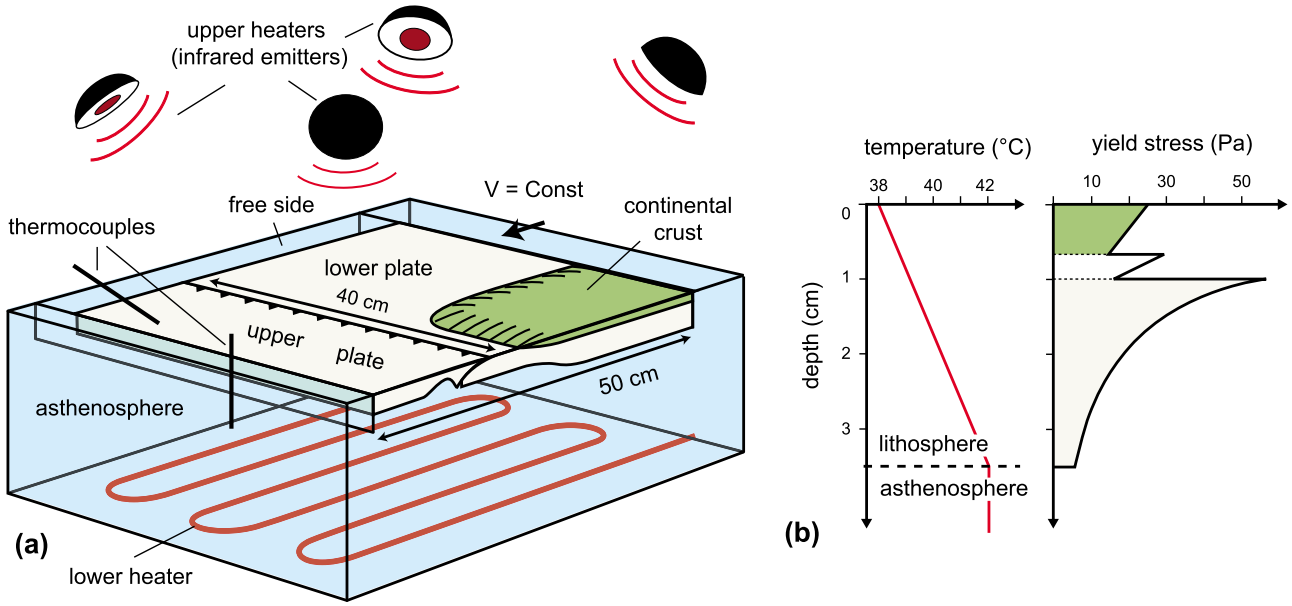

Figure 3. Three-dimensional sketch of the experimental setup. (a) Two lithospheric plates made of hydrocarbon materials rest on an asthenosphere modeled by water. Plate convergence is imposed at a constant rate. Model strain is monitored using a particle imaging velocimetry system imaging the model surface. A second camera is employed to follow the model evolution from the side. (b) A temperature gradient is imposed in the model lithosphere, producing a strength reduction with depth in each layer. In the presented experiments the model lithosphere is placed near the front wall. The gap between the model and the walls of the tank is ~5 mm in the front and 10 cm in the back.

generates trench-parallel compressive or tensile normal stresses, with poorly constrained effects on the mechanics of mountain building. It has been shown that local trench-parallel extension in a collision zone in a state of general compression locally changes the regime as the interplate pressure is locally reduced. As a result, rapid exhumation of the buoyant deeply subducted continental crust can occur [*Boutelier and Chemenda*, 2008]. However, it is not yet known how trench-parallel shortening/extension affects the continuity of the collision propagation.

[7] In terms of modeling strategy, we must clearly separate the effect of the gradient in nonhydrostatic normal push from that of horizontal drag of the fore arc by using three-dimensional experiments in which each effect can be isolated. The influence of the gradient in nonhydrostatic normal push is investigated here in experiments with no subduction obliquity that incorporate variations in the value of passive margin obliquity. The effect of the fore-arc horizontal drag is investigated independently in experiments in which the active and passive margins share the same orientation, oblique to the convergence direction. In this case there is no gradient in nonhydrostatic normal stress inside the collision zone but there is a horizontal shear drag that induces trench-parallel stress in the fore arc.

3. Modeling Technique

3.1. General Modeling Scheme

[8] The lithosphere is the outer shell of the Earth capable of undergoing large quasi-rigid horizontal displacements with strain rates far lower than those experienced by the underlying sublithospheric mantle [*Anderson*, 1995]. This definition provides the general framework for our modeling. The asthenosphere exerts a small shear traction on the base of the lithosphere. Integrated over the very large surface area of the base of a lithospheric plate, this traction becomes very important and must be taken into account when investigating the dynamics of the plate [*Funiciello et al.*, 2004; *Schellart*, 2004; *Bellahsen et al.*, 2005]. Since we do not investigate the dynamics of the plate but only the mechanics of plate deformation, we adopt a simpler kinematic framework in which we neglect the shear traction exerted by the asthenosphere on the lithosphere and replace its large-scale effect as a driving/resisting force of plate motion by a piston that imposes constant rate convergence between the lithospheric plates. Consequently, we model the asthenosphere with a low-viscosity fluid whose unique role is to provide hydrostatic equilibrium below the lithosphere.

3.2. Model Setup

[9] We employ a new 3-D thermomechanical apparatus [*Boutelier and Oncken*, 2011] based on earlier 2-D mechanical and thermomechanical experimental setups [*Boutelier et al.*, 2002, 2003, 2004; *Boutelier and Chemenda*, 2011]. The model includes two model lithospheric plates resting on the low-viscosity model asthenosphere (Figures 3a and 3b). The plates are made of temperature sensitive elastoplastic materials that are subjected to a constant vertical thermal gradient causing a strength reduction with depth in each layer (Figure 3b). The oceanic overriding plate comprises a single layer of analog mantle material that is thinner under the magmatic arc [*Tatsumi et al.*, 1983; *Furukawa*, 1993; *Zhao et al.*, 1994, 1997; *Schmidt and Poli*, 1998; *Ulmer*, 2001; *Kelemen et al.*, 2003; *Peacock*, 2003; *Currie et al.*,

Table 1. Parameter Values Adopted for the Model, Scaled to Nature and Scaling Factors[a]

Parameter	Value	Nature	Ratio
Upper crust thickness, H_{uc} (m)	6×10^{-3}	2.1×10^{4}	2.86×10^{-7}
Lower crust thickness, H_{lc} (m)	4×10^{-3}	1.4×10^{4}	2.86×10^{-7}
Continental lithospheric mantle thickness, H_m (m)	24×10^{-3}	8.4×10^{4}	2.86×10^{-7}
Upper crust yield strength, σ_{uc} (Pa)	19	2.16×10^{8}	8.8×10^{-8}
Lower crust yield strength, σ_{lc} (Pa)	21	2.39×10^{8}	8.8×10^{-8}
Continental lithospheric mantle yield strength, σ_m (Pa)	20	2.27×10^{8}	8.8×10^{-8}
Elastic shear modulus, G (Pa)	$\sim 1 \times 10^{3}$	$\sim 1 \times 10^{10}$	8.8×10^{-8}
Upper crust density, ρ_{uc} (kg m^{-3})	8.60×10^{2}	2.79×10^{3}	3.08×10^{0}
Lower crust density, ρ_{lc} (kg m^{-3})	8.60×10^{2}	2.79×10^{3}	3.08×10^{0}
Lithospheric mantle density, ρ_m (kg m^{-3})	1.0×10^{3}	3.25×10^{3}	3.08×10^{0}
Asthenospheric mantle density, ρ_a (kg m^{-3})	1.0×10^{3}	3.25×10^{3}	3.08×10^{0}
Thermal diffusivity, κ (m^2 s^{-1})	2.8×10^{-8}	1.0×10^{-6}	2.8×10^{-2}
Velocity, V (m s^{-1})	1.245×10^{-4}	1.27×10^{-9}	9.8×10^{4}
Time, t (s)	9.2×10^{1}	3.15×10^{13}	2.92×10^{-12}

[a]The plastic strength of the materials decreases with depth in each layer. We indicate the strengths averaged over the layer thickness. The elastic shear modulus is only approximately scaled. The mechanical properties of the materials, measurements, and experimental setup and scaling are detailed by *Boutelier and Oncken* [2011].

2004, 2008]. The frontal tip of this plate is made of a weaker material representing the accretionary wedge. The subducting plate comprises two parts. The first part is oceanic and made of one single layer of mantle lithosphere material. The second part is a continental analog comprising three layers: the upper crust, the lower crust and the lithospheric mantle. Between the continental and oceanic domains is a continental passive margin where the thicknesses of the crust and lithospheric mantle reduce progressively toward the oceanic domain (Figure 3a). The temperature at the model surface is maintained at 38°C while the temperature of the asthenosphere layer is 42°C. This results in a conductive temperature gradient in the model lithosphere prior to deformation, giving a smooth rheological stratification (Figure 3b). A piston moving at a constant rate imposes the convergence velocity, which is chosen in order to scale with the heating rate during subduction and the weakening of the model material during this process [*Chemenda et al.*, 2000a; *Boutelier et al.*, 2002, 2003, 2004; *Boutelier and Chemenda*, 2011]. In order to monitor the model deformation from the side, the model lithosphere is placed next to the sidewall of the experimental tank on one side (the gap is 5–10 mm), while on the other side the model oceanic lithosphere ends ~10 cm from the wall providing space for motion in this direction. The side views are only used for qualitative analysis of the model deformation while surface views are used for quantitative strain monitoring using Particle Imaging Velocimetry [*Adam et al.*, 2005; *Hoth et al.*, 2006; *Schrank et al.*, 2008; *Riller et al.*, 2010; *Boutelier and Oncken*, 2011].

3.3. Model Scaling

[10] The principle of analog modeling is based on scaling laws, in which geometric, kinematic and dynamic similarity between the natural prototype and the model are achieved by scaling down lengths, time, and forces [*Buckingham*, 1914; *Hubbert*, 1937; *Ramberg*, 1967; *Davy and Cobbold*, 1991; *Shemenda*, 1994]. When scaling relationships are fulfilled, the model behaves mechanically like the prototype but is manageable in a laboratory, and the effects of various key parameters can be tested using multiple, carefully designed, built and monitored experiments.

[11] The scaling relationships (i.e., dimensionless ratios of parameters relevant to the investigated phenomena) employed for the scaling of the experiments here are the following: H_{uc} / H_{lc} = const, H_{lc} / H_{lm} = const, σ_{uc} / $\rho_{uc}gH_{uc}$ = const, σ_{lc} / $\rho_{lc}gH_{lc}$ = const, σ_{lm} / $\rho_{lm}gH_{lm}$ = const, ρ_{uc} / ρ_{lc} = const, ρ_{lc} / ρ_{lm} = const, ρ_{lm} / ρ_a = const, VH / κ = const, Vt / H = const, where H_{uc}, H_{lc}, H_{lm}, and H are the thicknesses of the upper crust, lower crust, lithospheric mantle, and entire lithosphere, respectively; ρ_{uc}, ρ_{lc}, ρ_{lm}, and ρ_a are the densities of the upper crust, lower crust, lithospheric mantle, and asthenosphere, respectively; σ_{uc}, σ_{lc}, and σ_{lm} are the yield strengths averaged over the layer thickness for the upper crust, lower crust, and lithospheric mantle, respectively; g is the gravitational acceleration; V is the convergence rate; t is the time; and κ is the thermal diffusivity of the lithosphere.

[12] For convenience the model lithosphere must be relatively small. Hence, we adopt 1 cm in the model representing 35 km in nature, which yields a length scaling factor $L^* = L_m/L_n = 2.86 \times 10^{-7}$. The scaling of all densities in the model is set by our choice of using water to represent the asthenosphere. The scaling factor for densities is therefore $\rho^* = \rho_m/\rho_n = 3.08 \times 10^{-1}$ since 1000 kg m^{-3} in the model represents 3250 kg m^{-3} in nature. Consequently, a neutrally buoyant lithospheric mantle is modeled by material with a density of 1000 kg m^{-3}, while the low-density continental crust is modeled by material with a density of 860 kg m^{-3} representing 2795 kg m^{-3} in nature. The hydrostatic pressure, ρgz, where depth z scales with length, sets the scaling of stress. Since the experiments are produced with normal gravitational acceleration (i.e., $g^* = 1$ or $g_m = g_n = 9.81$ m s^{-2}), $\sigma^* = \sigma_m/\sigma_n = \rho^* \times L^* = 8.79 \times 10^{-8}$, a flow stress of ~10 MPa at the bottom of the lithosphere must be ~1 Pa in the model, while a flow stress of ~500 MPa in the stronger parts of the lithosphere corresponds to ~45 Pa in the model. Since the strength decreases within each layer because of the temperature increase, we employ the strength averaged over the layer thickness for the scaling. The upper crust and lithospheric mantle layers have an average yield strength of ~19 Pa, which corresponds to ~216 MPa in nature. The lower crust is slightly stronger, with an average yield strength of ~21 Pa corresponding to 239 MPa in nature, but yield strength reduces strongly with depth within this layer (Figure 3b). With a stronger lower crust, we implement two

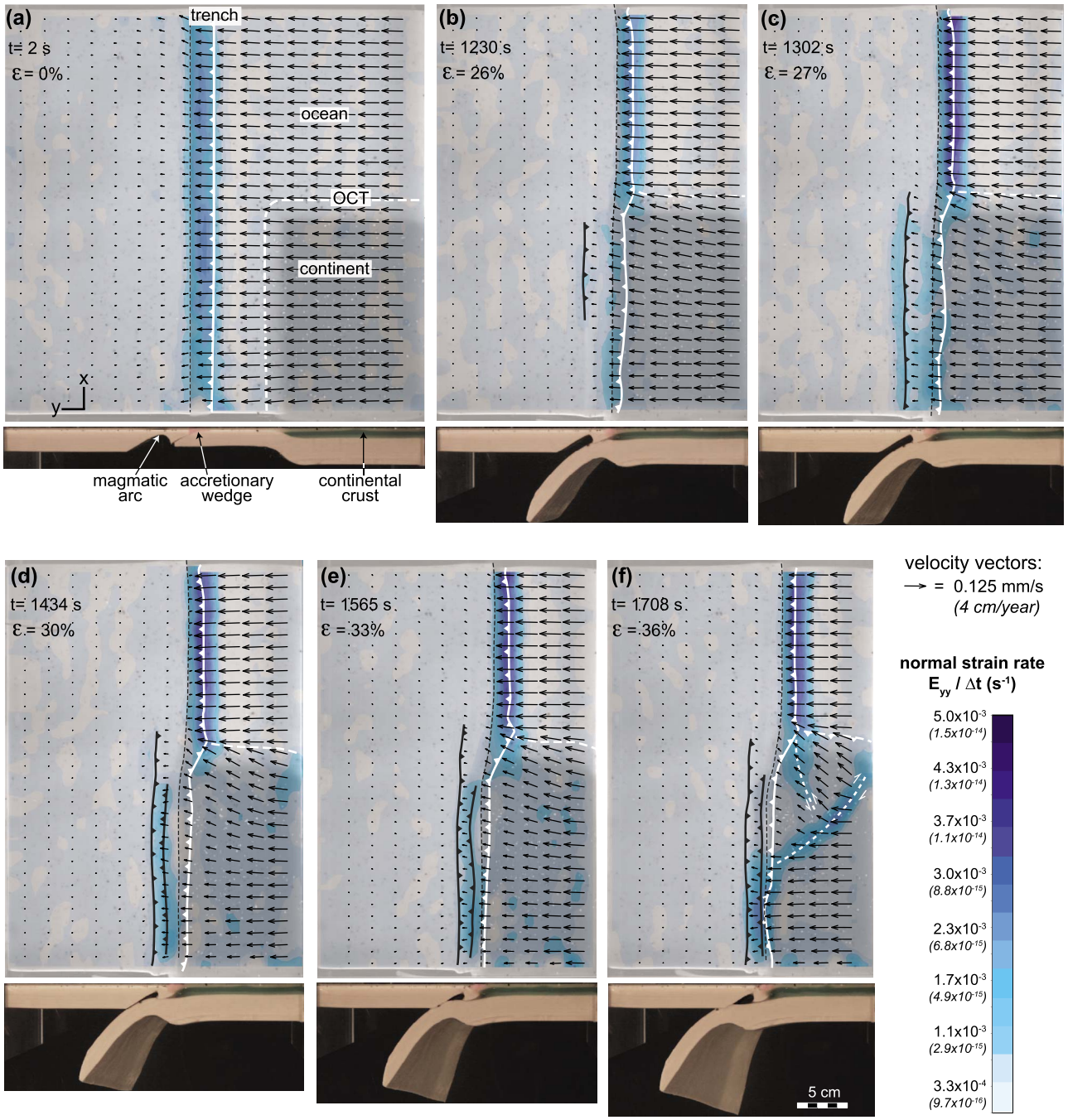

Figure 4. Successive views of Experiment 1. For each stage we present the side view and the surface view with velocity vectors derived from cross correlation of successive images and scaled-up convergence-parallel strain rate $E_{yy}/\Delta t$. (a) Oceanic subduction. (b and c) Initial collision. Accretionary wedge is backthrusted and a fault is created in the arc area dipping toward the continent. (d and e) Subduction of the fore-arc block. The fault zone in the arc becomes inactive and a new one is created in front of it that dips toward the ocean. (f) Deformation of the passive margin, including shortening in the convergence-parallel direction with vertical thickening near the right-hand side and horizontal extrusion near the transition between collision and subduction.

possible low-strength horizons (décollements) into which thrusts may root: at the interface between the upper and lower crust, and at the interface between the lower crust and the lithospheric mantle.

[13] The scaling of time is chosen in order to scale the temperature variations associated with deformation. The imposed velocity controls the advection of heat in the model, which must be balanced by the diffusion. In order to maintain the same balance between advection and diffusion as in nature, the dimensionless ratio VL / κ must be the same in the model and nature [*Chemenda et al.*, 2000a]. Since the scaling of length is already set, the thermal diffusivity of the

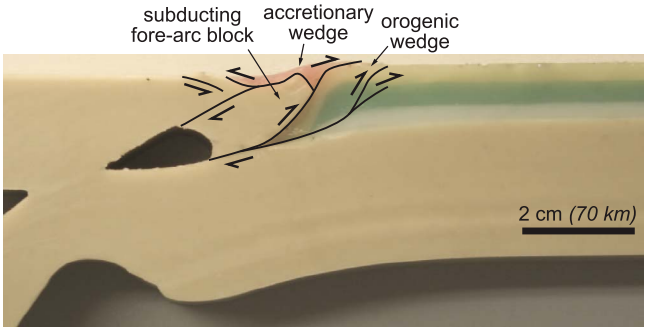

Figure 5. Postdeformation cross section of the frozen model lithosphere in the middle of the collision zone. The accretionary wedge (pink) is thrusted over the fore-arc block, which is subducted under the arc. The continental passive margin is shortened and thickened.

analog materials controls the scaling of velocity and therefore of time. The latter is simply defined in a kinematic sense using the dimensionless ratio Vt/L. Our new hydrocarbon-based compounds have a thermal diffusivity of 2.8×10^{-8} m^2 s^{-1} [*Boutelier and Oncken*, 2011]. Assuming that natural rocks have a thermal diffusivity of 1×10^{-6} m^2 s^{-1} [*Turcotte and Schubert*, 1982], then $\kappa^* = 2.8 \times 10^{-2}$, giving a scaling factor for velocity $V^* = V_m/V_n = \kappa^*/L^* = 9.8 \times 10^4$. This scaling factor means that a natural convergence velocity of 4 cm yr^{-1} (i.e., 1.27×10^{-9} m s^{-1}) is 0.125 mm s^{-1} in the model. The scaling factor for time is therefore $t^* = t_m/t_n = L^*/V^* = 2.92 \times 10^{-12}$, which implies that 1 Ma in nature (i.e., 3.15×10^{13} s) is 92 s in the model. The parameter values assumed for the prototype and the model are summarized in Table 1.

4. Results

[14] Multiple experiments have been conducted with various initial and/or boundary conditions. We present below details of the two most representative experiments and summarize the results from the others. In the first experiment we investigate the effect of the largest possible gradient of horizontal compression obtained when the edges of the continental passive margin vary in orientation by 90° (Figures 3a and 4a). Therefore the location of the transition between collision and subduction is fixed in space and the gradient of trench-perpendicular compression increases progressively with time (or more precisely, with the amount of continental subduction, which increases with time). In the second experiment, the location of the transition between collision and subduction is also fixed in space but the experiment also investigates the effect of a relatively large subduction obliquity angle (30°).

4.1. Experiment 1: Passive Margin Obliquity Angle

[15] The experiment began with subduction initiation along a predefined interplate zone (Figure 4a) followed by subduction of the oceanic lithosphere. During these initial stages, the overriding plate was not deformed except for within the accretionary wedge (Figure 4a). Displacement vectors from PIV monitoring of the model surface show that plate convergence was accommodated in the subduction zone without significant deformation of the plates (Figure 4a), as in previous 3-D thermomechanical oceanic subduction experiments [*Boutelier and Oncken*, 2011]. When the continental passive margin was being subducted, a part of the accretionary wedge was backthrusted over the fore-arc block while another was subducted (Figures 4b and 4c). At the transition between collision and subduction, the accretionary wedge sheared rapidly parallel to the convergence direction in the horizontal plane. Horizontal compression due to subduction of the buoyant continental crust then led to failure of the overriding plate in the arc area (Figures 4 and 5). The first fault created in the arc area dipped toward the subducting continental plate (Figure 4c). Such faults generally lead to subduction polarity reversal [*Chemenda et al.*, 2001; *Boutelier and Chemenda*, 2011]. However, this fault was rapidly abandoned and a new oceanward dipping fault was created in the frontal part of the arc area, which led to subduction of the fore-arc block (Figures 4d and 5). These two faults propagated rapidly across the entire length of the collision zone and into the transition zone between collision and subduction (Figure 4). With increasing convergence and thus quantity of subducted continental crust, the seaward dipping fault in the arc did not cut through the fore arc but instead remained in the arc area and propagated laterally into the transition zone. The fore arc is subducted in this zone, despite the lack of push by subducting continental crust and was, as expected, sheared parallel to the convergence direction in the horizontal plane. However, this shearing does not evolve into one single narrow zone of high strain. Instead, shear strain was diffused over a relatively large area resulting in a relatively low magnitude of shear strain. The process of fore-arc block subduction was interrupted by failure of the continental crust in the subducting margin, which led to formation of an orogenic wedge in the collision zone (Figures 4 and 5) and a strike-slip system that accommodated horizontal extrusion of the continental crust near the transition zone (Figure 4f). Convergence was then taken up by these crustal structures and continental passive margin and fore-arc block subduction ceased. The experiment was stopped at this stage and the model cooled in order to produce cross sections (Figure 5).

4.2. Experiment 2: Passive and Active Margins Obliquity Angles

[16] The effect of the subduction obliquity angle θ was tested in Experiment 2 (Figure 6). The model included an initial subduction obliquity angle of 30° (Figures 6a and 6b). This relatively large subduction obliquity angle was expected to trigger strain partitioning and lateral (i.e., trench-parallel) migration of the fore-arc block during its subduction [*Fitch*, 1972; *Beck*, 1983; *Jarrard*, 1986; *Chemenda et al.*, 2000b]. Such lateral motion of a fore-arc sliver requires trench-parallel shortening or extension of the fore arc near the termination of the sliver [*Jarrard*, 1986; *Avé Lallemant and Guth*, 1990; *Beck*, 1991; *Beck et al.*, 1993]. We designed the model lithosphere to promote trench-parallel extension in the transition zone between collision and subduction. Together with the convergence-parallel shearing due to the compression gradient, this trench-parallel extension was expected to result in a transtensional deformation of the fore-arc block in this zone.

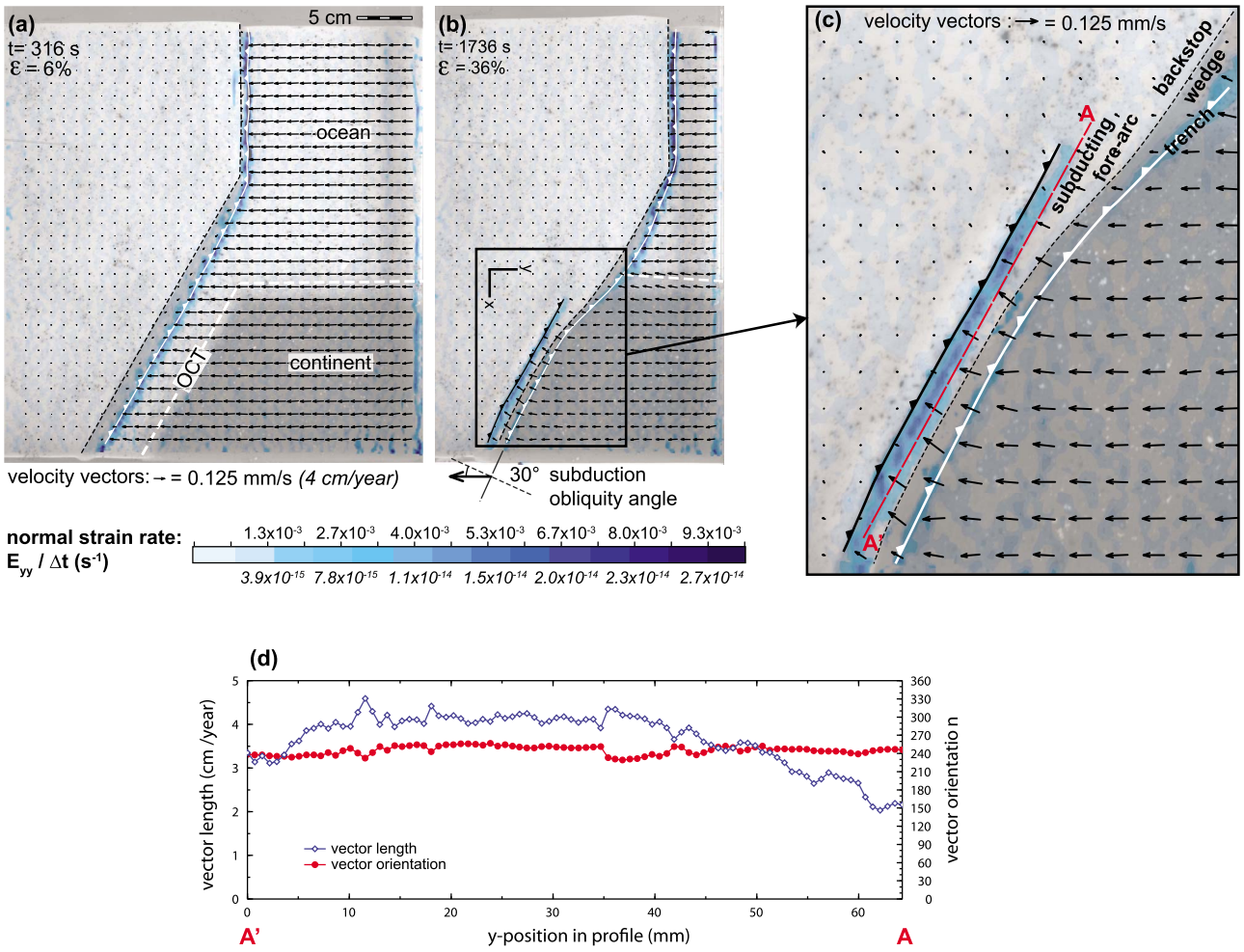

Figure 6. Model surface views in Experiment 2 with velocity vectors derived from cross correlation of successive images and scaled-up convergence-parallel strain rate $E_{yy}/\Delta t$. (a) Oceanic subduction, (b) arc-continent collision with subduction of the fore-arc block, (c) close-up of the subduction-collision transition zone showing the motion of the fore-arc block perpendicular to the strike of the trench, and (d) profile of velocity magnitude and orientation along the subducting fore arc (see Figure 6c for location), showing no rotation about a nearby vertical axis.

[17] In this experiment, oceanic subduction prior to collision resulted in strain partitioning with trench-parallel horizontal shearing of the accretionary wedge (Figure 6). However, the basement of the fore arc was not dragged laterally during this stage. Subduction of the continental passive margin resulted in substantial subduction of the accretionary wedge (i.e., subduction erosion) and failure of the overriding lithosphere along an oceanward dipping fault in the arc area. This was followed by subduction of the fore-arc block with diffuse trench-normal simple shearing of the fore-arc block in the subduction-collision transition zone (Figure 6). The horizontal displacement of the fore arc during its subduction was perpendicular to the trench (Figure 6c); the fore-arc block was not dragged laterally along the trench despite the imposed high obliquity angle. In the collision zone, the velocity vectors in the subducting fore-arc block did not decrease in magnitude away from the transition zone, nor did their orientation change along strike (Figure 6d). This proves that there was no wholesale rotation of the subducting fore arc into the new subduction but rather a normal push that did not vary significantly along strike.

4.3. Other Experimental Results

[18] In other experiments we varied the following parameters: (1) the strength of the arc lithosphere, (2) the strength of the passive margin, (3) the initial geometry of the passive margin in map view, and (4) the lateral boundary condition.

[19] These experiments generally resulted in deformation of the weak arc lithosphere with diffuse horizontal trench-normal simple shearing of the fore arc in the transition zone, as observed in Experiments 1 (Figures 4 and 5) and 2 (Figure 6). No experiments generated a narrow zone of high strain crosscutting the fore arc. Here we describe qualitatively the observed impact or lack of impact of the parameters above.

[20] We varied the strength of the arc lithosphere by changing its thickness, the surface temperature and by

including or omitting a weak arc crust. The strength of the arc lithosphere controls the relative timing of its failure. A strong arc lithosphere generally fails later than a weak one, when more buoyant continental crust has been subducted. The style of deformation and the propagation mechanism, however, are similar. We observed that the presence of a weak arc crust may localize the fault, which nucleates in the weakest part of the model lithosphere, at the base of the arc crust.

[21] By varying the surface temperature we changed the model strength at the surface and thus the strength of the subducted margin. A weak passive margin deforms earlier than a strong one (i.e., when little crust has been subducted). Subduction of the fore-arc block can subsequently be interrupted at any moment by failure of the crust in front of the subduction zone. Both the timing of failure of the arc lithosphere (i.e., beginning of fore-arc subduction or subduction reversal) and the timing of failure of the continental crust (which interrupts fore-arc subduction) depend on the relative strengths of the arc and continental crust as well as the magnitude of compressive stress generated by subduction. The latter clearly depends on multiple parameters including slab pull, crustal buoyancy and the flexural rigidity of the subducted lithosphere, as well as parameters linked to viscous coupling between the subducted slab and surrounding mantle. We cannot precisely predict the conditionals leading to and timing of crustal failure using the current modeling technique because it depends on a too large number of poorly constrained variables and some important effects (i.e., viscous coupling in mantle) are not yet implemented in the experimental setup. We conclude that within the range of realistic parameter values all failure scenarios (i.e., early versus late arc failure or no arc failure) are possible.

[22] Experiment 1 (Figures 4 and 5) had the largest possible horizontal gradient of horizontal compression since it was imposed over the smallest possible distance along the trench (i.e., the width of the passive margin) (Figure 2). Prior to performing this experiment, we tested the effect of obliquity angles 30° and 60°. For both experiments we obtained the same deformation scenario as detailed for Experiment 1. Since the same process is observed regardless of obliquity angle, there is no threshold gradient of trench-perpendicular compression that leads to formation of a strike-slip fault zone through the fore arc.

[23] Finally, we tested two alternative lateral boundary conditions. In Experiments 1 and 2 side views were obtained because the model edge and the sidewall were only separated by a small (5–10 mm) gap of hot water, which prevented lateral flow. This provided a pseudo free-slip boundary condition because the model lithosphere cannot move toward the wall but can easily move parallel to it. Deformation of the model lithosphere near the sidewall was not strictly identical to that occurring in the middle of the collision zone but the difference was small and this experimental setup permitted monitoring of the collision in vertical cross section. In another setup both edges of the model continental lithosphere thinned progressively before reaching the edges of the model plate. In this situation the continental crust was not in contact with hot water along the edges of the model plate and the side views only displayed subduction of the oceanic lithosphere. The model lithosphere was then placed in the center of the tank with a large gap (5 cm) on both sides and was free to move toward or parallel to the sidewalls. Since we observed the same deformation mechanisms of the arc lithosphere and passive margin with both boundary conditions, only experiments with the model close to the sidewall, which provided vertical views, have been presented.

5. Discussion

5.1. Failure of the Arc Lithosphere in the Subduction-Collision Transition Zone

[24] The pattern and evolution of deformation in our experiments suggest a scenario of arc-continent collision that is similar to that obtained in earlier 2-D mechanical and thermomechanical experiments [*Chemenda et al.*, 2001; *Boutelier et al.*, 2003] in that (1) the subduction of the continental passive margin generates a strong horizontal compression of the upper plate, (2) this compression leads to failure of the arc lithosphere and fore-arc block subduction, and finally (3) this process is interrupted by the failure of the continental crust in front of the subduction zone.

[25] The experimental results also provide new insights on the lateral termination of the collision zone. In the subduction-collision transition zone, the fault within the arc lithosphere that accommodates subduction of the fore-arc mantle block does not propagate toward the main subduction thrust through the fore arc. We hypothesized that this mechanism might arise when the trench-parallel horizontal gradient of trench-perpendicular compression is sufficiently large. However, our experiments never produced a strike-slip fault system cutting through the fore arc even for the largest possible gradient of trench-perpendicular compression obtained when the strike of the subducted passive margin turns by 90°. The reason for this is that the fault in the arc propagated within the transition zone but remained in the arc area because the lithosphere there is thin, hot and mechanically weak. Additionally, the arc lithosphere in the transition zone did not fail because of trench-perpendicular compression caused by the buoyancy of the thin continental crust of the subducted continental passive margin but rather because of drag exerted by the subducting fore-arc block in the neighboring segment of the plate boundary. If the arc lithosphere is very thin and weak, the fault zone can propagate outside the transition zone into the part of the plate boundary where oceanic lithosphere is being subducted. In this situation there is no push on the interplate zone due to the buoyancy of the subducted crust and shortening must be generated by drag exerted by the subducting fore-arc block in the neighboring segment of the plate boundary where collision is occurring (Figures 4 and 6). Trench-parallel propagation of the arc fault then prevents the formation of a strike-slip system through the fore-arc domain. In the transition zone, the fore-arc block is sheared in the horizontal trench-perpendicular direction, but because of the fault that has propagated in the arc, the shear strain is diffused across a large area and does not localize (Figures 4 and 6). This process is similar to the deformation of the oceanic lithosphere when it enters the subduction zone. The plate bends down and deforms both elastically and plastically but the amount of deformation is not sufficient to produce a lithospheric scale zone of localized high strain throughout the entire thickness of the plate. These zones can only be produced if the plate or

in our case the fore-arc block is forced to bend with a very small curvature radius (i.e., high shear strain) [*Shemenda*, 1994]. However, in our experiments this scenario was prevented by the propagating failure of the arc lithosphere in the transition zone, which keeps the deforming area large and shear strain low.

[26] One may therefore hypothesize that the strength of the arc lithosphere controls how far the arc fault extends within the transition zone. If the fault cannot propagate laterally because the strength of the arc lithosphere is too high, then the horizontal trench-perpendicular shearing of the fore-arc block in the transition zone will be less diffused and could potentially lead to the formation of a narrow shear zone. However, if the thin and hot arc lithosphere remains weaker than the thick and cold core of the fore-arc block then a similar propagation of the fault occurs only the onset of failure is delayed. Furthermore, if the strength of the arc lithosphere is too high then the process of fore-arc block subduction is prohibited and convergence is accommodated directly by deformation of the continental crust in front of the subduction zone [*Chemenda et al.*, 1995; *Kaus et al.*, 2008; *Yamato et al.*, 2009].

5.2. Obliquity of Convergence Prior to and During Collision

[27] On our experiments the fore-arc block was too strong compared to the thin, hot and weak arc lithosphere to be dismembered because of the gradient in trench-normal compression along the trench. However, in nature the fore arc can be stretched as in the Sunda straight between the islands of Sumatra and Java [*Huchon and Le Pichon*, 1984; *Malod et al.*, 1995; *Susilohadi et al.*, 2009], the Mona rift between the islands of Hispaniola and Puerto Rico along the northern branch of the Caribbean subduction system [*van Gestel et al.*, 1998; *Jansma and Mattioli*, 2005] and in the Gulf of Guayaquil–Tumbes Basin in Ecuador-Peru [*Moberly et al.*, 1982; *Witt et al.*, 2006; *Witt and Bourgois*, 2009]. However, in these locations, fore-arc block deformation is not caused by the gradient of normal stress on the plate boundary, but rather by strain partitioning due to a high subduction obliquity angle. When this angle is sufficiently large, the fore-arc block can be dragged laterally along the trench [*Fitch*, 1972; *Chemenda et al.*, 2000b] and the displacement of this sliver is accompanied by trench-parallel extension and shortening at its ends [*Avé Lallemant and Guth*, 1990; *Beck et al.*, 1993]. In this situation the relative strength of the fore-arc block and arc lithosphere are not important because the trench-parallel deformation only involves the fore arc, which is decoupled from the arc/back arc by a strike-slip system. The weakness of the arc lithosphere actually assists the fore-arc deformation process by allowing the development of a strike-slip system (e.g., Central Sumatra fault, Figure 1).

[28] Our experiments reveal that the mechanism of fore-arc lateral migration is unlikely to play a significant role during arc-continent collision because it is the pressure force due to the buoyancy of the subducted continental margin, not the shear traction, that drives the motion of the fore arc. This is because the subduction of the continental crust leads to subduction erosion of the accretionary wedge during the initial stages of continental subduction, which lubricates the interplate zone and diminishes the shear traction. Furthermore, a blanket of sediment generally covers the subducted passive margin [*Reston and Manatschal*, 2011], which can be partially accreted and subducted [*Boutelier et al.*, 2002, 2004], and provides additional lubrication in the interplate zone. Therefore, there is an increase in pressure force and decrease in shear traction during subduction of the passive margin.

[29] However, the role of fore-arc lateral migration during arc-continent collision should not be entirely ignored. One new scenario that arose from our experimental results is that fore-arc lateral migration may have been initiated during the oceanic subduction stage prior to collision. In this case, it is possible that a preexisting rift within the fore-arc block can be reactivated during the collision.

[30] One example of such a scenario may apply to the westward propagation of the Timor arc-continent collision where the Australian continental lithosphere is being subducted beneath the Banda block [*Silver et al.*, 1983; *Snyder et al.*, 1996; *Bock et al.*, 2003; *Harris*, 2011]. The resulting horizontal compression has resulted in the formation of the Wetar and Flores thrusts (Figure 1) behind the magmatic arc [*Genrich et al.*, 1996; *Snyder et al.*, 1996]. Near the transition between collision and subduction, the fore-arc block is presently being sheared in the horizontal trench-normal direction but GPS data do not indicate a sharp boundary (Figure 1) [*Nugroho et al.*, 2009] but rather a diffuse shearing as observed in our experiments (Figures 4 and 7). Because of the obliquity of the convergence and shape of the active and passive margins, the collision is propagating westward. However, toward the west the trench turns north and the obliquity of the convergence increases. As a result, strain partitioning associated with oblique oceanic subduction has led to the formation of the Central Sumatra fault that accommodates northward motion of the fore arc in Sumatra (Figure 1). Between the islands of Sumatra and Java, where the trench turns sharply north, strain partitioning led to the formation of the Sunda straight, which accommodates trench-parallel extension on normal faults that cut through the fore arc [*Huchon and Le Pichon*, 1984; *Malod et al.*, 1995; *Susilohadi et al.*, 2009]. On the basis of our experimental results, we speculate that the arc-continent collision in Timor will propagate westward in a continuous manner until deformation behind or in front of the magmatic arc reaches the Sunda straight. This preexisting major zone of weakness within the fore arc may then lead to discontinuous propagation of the arc-continent collision. We conclude that consideration of first-order three-dimensional structures inherited from the early stages of oceanic subduction, prior to collision, are critical for understanding the mechanics of arc-continent collision.

5.3. Evolution of Interplate Stress Conditions During Subduction of the Continental Margin

[31] We have demonstrated that fore-arc block motion is perpendicular to the trench during subduction of a continental margin. We argue that this occurs because interplate zone shear traction is reduced because of the entrainment of passive margin cover sediments and subduction erosion of the accretionary wedge. The nonhydrostatic normal stress also increases because of buoyancy of the subducted continental margin. This evolution of stress conditions is fundamental for exhumation of the subducted continental

crust. Previous three-dimensional thermomechanical experiments found that a local reduction of interplate pressure is required to allow buoyancy-driven exhumation of deeply subducted ultrahigh pressure nappes between the plates [*Boutelier and Chemenda*, 2008]. In these models, reduction of interplate pressure was achieved via an artificially imposed trench-parallel extension in the upper plate and it was proposed that this could be a natural effect caused by curvature of the plate boundary. Investigating this hypothesis, 2-D numerical simulations of the stress field generated in the upper plate by various stress conditions imposed on a curved plate boundary revealed that trench-parallel extension can only be produced near the symmetry axis of a concave-seaward plate boundary if the shear traction is low compared to the nonhydrostatic normal stress [*Boutelier and Oncken*, 2010]. Conversely, during oceanic subduction with low nonhydrostatic normal stress and possibly large shear traction, trench-parallel compression can result in the upper plate if the plate boundary is concave seaward. Upper plate trench-parallel

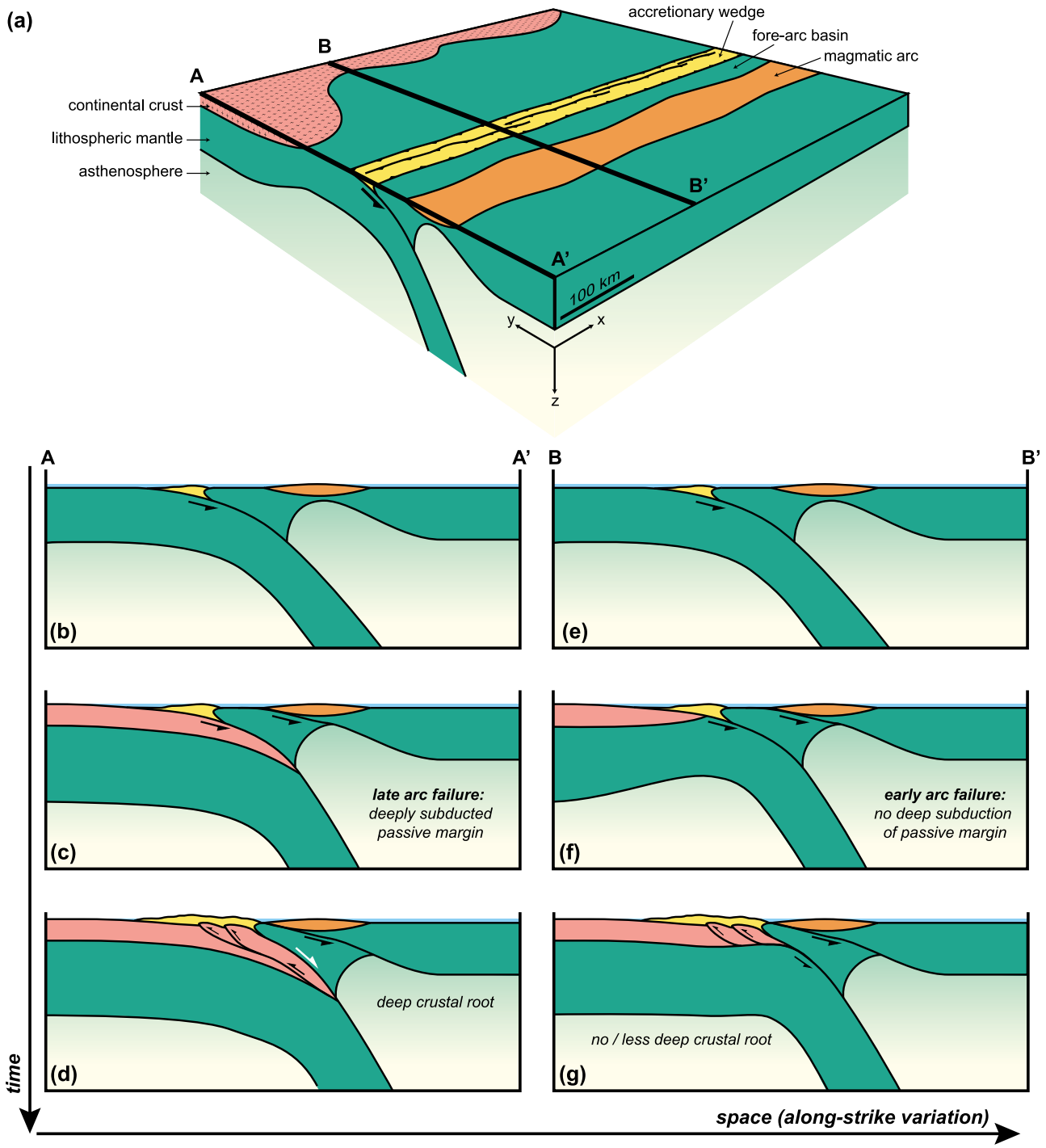

Figure 7

extension during continental subduction is therefore predicted under conditions of high nonhydrostatic normal compression and reduced shear traction. Our experimental results show that these are the conditions associated with continental subduction. It follows that continental subduction along a concave-seaward plate boundary following oceanic subduction may produce a switch from trench-parallel compression to trench-parallel extension, which allows local reduction of the interplate pressure and buoyancy-driven exhumation of the subducted continental crust [*Boutelier and Chemenda*, 2008].

5.4. Impact of Early Fore-Arc Subduction on the Depth of Continental Subduction

[32] Our experimental results demonstrate that deformation in the arc associated with the subduction of the continental margin can be advanced or delayed depending on the degree and sense of lateral coupling between adjacent segments of the plate boundary. During initial contact between the arc and the passive margin, the arc is laterally connected to segments of the plate boundary not yet undergoing continental subduction. Oceanic subduction in the two neighboring segments may result in weak compression or tension [*Shemenda*, 1994; *Boutelier and Chemenda*, 2011]. The fore arc may therefore not be actively dragged downward in each neighboring segment. It follows that the coupling with the segment experiencing continental subduction is resistive in nature. As a result fore-arc subduction initiates later than in 2-D models where the force arising from this resistive coupling is neglected.

[33] Similarly, once the collision is initiated and is propagating laterally, the segment experiencing the early stage of the collision (i.e., in the subduction-collision transition zone where the passive margin is just starting to be subducted) is adjacent on one side to a segment where the collision is advanced and the fore-arc block subduction process has started. Consequently, one of the couplings between the neighboring segments is now driving fore-arc block subduction, while the other is resisting. As a result fore-arc subduction initiates earlier than in 2-D models. A further consequence is that the sense of failure in the arc (i.e., a fault dipping toward the continent or the ocean) tends to propagate laterally. Without along-strike variations of the initial conditions, the prevailing sense of failure should be the one that developed when the plates initially collided. However, this is true only when one sense of failure clearly dominates during initial collision. In multiple experiments, the initial deformation of the arc lithosphere included both fault directions, and during these early stages the polarity can change quickly.

[34] The along-strike coupling effect is very similar to that described in sand wedge experiments [*Schreurs et al.*, 2006], which find that thrusts are convex or concave toward the hinterland in map view depending on whether shortening is induced by a mobile backwall or conveyer belt (i.e., fixed backwall), respectively. This occurs because the sense of shear stress along the sidewalls is different for fixed versus mobile backwall experiments. In mobile backwall models the shear traction along the sidewalls is in the same direction as the basal traction. Consequently the traction driving the sand wedge up and the resulting taper angle are greater than for the case of fixed backwall models [*Schreurs et al.*, 2006]. This effect can only be observed in three-dimensional experiments as the traction along the sidewall or, in our case, the coupling between adjacent segments of the plate boundary cannot be included in two-dimensional models [*Kaus et al.*, 2008; *Yamato et al.*, 2009; *Dymkova et al.*, 2010; *Afonso and Zlotnik*, 2011]. However, numerical simulations offer other advantages. For example, using 2-D and 3-D numerical simulations *van Hunen and Allen* [2011] and *Afonso and Zlotnik* [2011] demonstrated the importance of the dynamical aspects of the collision process by showing that a reduction in plate convergence impacts the thermal structure of the subducted slab, leading to slab break off. This process must certainly influence the deformation in the arc area. In addition, a dynamic collision may also result in a change in plate motion direction [*Bellahsen et al.*, 2003], which will also fundamentally change the deformation in the arc area. However, the effect of changes in plate motion direction can only be investigated in three-dimensional experiments.

[35] The relative timing of failure in the arc changes during collision propagation, which has a profound consequence on the depth to which the passive margin can be subducted. This is because convergence may be solely accommodated by the new subduction zone beneath the magmatic arc once fore-arc block subduction has been initiated, at which point passive margin subduction ceases [*Boutelier et al.*, 2003]. Finally, the fore-arc block may be entirely subducted [*Boutelier et al.*, 2003], or it can stop at

Figure 7. Sketch illustrating the structural variations arising because of coupling between neighboring segments of the plate boundary. (a) Three-dimensional block diagram showing an arc-continent collision initiating at point A and propagating to point B. (b–d) Evolution in time of the arc-continent collision in vertical section A–A′. Figure 7b shows the initial stage of oceanic subduction. Figure 7c shows that during initial contact between the plates, fore-arc subduction is resisted by coupling between neighboring segments where oceanic subduction occurs. Consequently, arc failure and fore-arc block subduction initiate late, when the passive margin is already deeply subducted. Figure 7d shows that the process is interrupted by failure of the continental crust in front of the orogen, which also occurs late within the process of arc-continent collision. (e–g) Evolution in time of the arc-continent collision in vertical section B–B′. Figure 7e shows the initial stage of oceanic subduction, similar to Figure 7b. Figure 7f shows that during subduction of the continental margin, failure of the arc lithosphere and subduction of the fore-arc block occurs early because of along-strike coupling with section A–A′ where fore-arc subduction is already ongoing. Consequently, the passive margin is not deeply subducted. Figure 7g shows that the failure of the crust in front of the orogen also propagates rapidly from A–A′ to B–B′. Subduction of the fore-arc block and the continental passive margin ceases as convergence is now accommodated in these structures. The orogen in section B–B′ did not develop a deep crustal root. The structural variations between sections A–A′ and B–B′ are exaggerated for clarity.

an early stage when the stress required to continue downward motion is balanced by the strength of the crust in front of the collision zone. At this point convergence is accommodated by thick-skinned and thin-skinned deformation of the crust in front of the suture zone. It follows that if deformation of the arc and passive margin intervene at an earlier stage of the arc-continent collision process than observed in previous 2-D experiments [*Boutelier et al.*, 2003; *Dymkova et al.*, 2010], then subduction of the passive margin may cease at an early stage and at shallow depth (Figure 7). Our results suggest that the initial contact between the passive margin and the arc may result in deeper continental subduction than in 2-D models or at later stages when the collision propagates laterally (Figure 7). The results therefore predict an asymmetry within the structure of the orogenic belt and associated metamorphic conditions, with higher pressure conditions occurring close to the initiation point of the collision.

6. Conclusions

[36] Using a three-dimensional thermomechanical modeling technique we have demonstrated that, in the absence of inherited weak zone, the gradient in nonhydrostatic normal stress generated by a propagating arc-continent collision does not produce a strike-slip fault zone within the fore arc. Our experiments further showed that motion of the fore arc is driven by normal nonhydrostatic normal stress and that the effect of shear traction is minor during collision. Consequently, trench-parallel extension cannot be generated simply because of obliquity of the collision but requires that the plate boundary is concave seaward. However, the experiments suggest that if the upper plate acquires structures due to trench-parallel extension during the initial stages of oceanic subduction, these structures may be reactivated during collision.

[37] However, in the absence of preexisting major zones of weakness inherited from subduction history, the lithospheric scale fore-arc deformation is continuous along the strike of the orogen. This suggests that the deformation mechanism is constant during collision propagation and that, in this case, the space for time substitution hypothesis is valid. However, the modeling results also show that deformation is three-dimensional and that ongoing deformation in adjacent segments of the plate boundary strongly influences the relative timing of deformation. Therefore, even though deformation mechanisms are similar along the strike of the plate boundary, early or delayed timing of failure results in progressive structural variations in the belt. Comparing our experiments to previous two-dimensional models, failure is delayed during initial contact between the plates but is advanced when the collision propagates laterally. This can result in deeper subduction of the continental margin during the initial stages of collision. The results predict that orogenic belts are likely to have an asymmetric structure with a deeper crustal root and higher metamorphic pressures recorded in exhumed rocks closer to the location of initial plate collision.

[38] **Acknowledgments.** We thank M. Rosenau, F. Neumann, and T. Ziegenhagen for support, engineering, and technical assistance. We thank J. Malavielle and S. Haq for constructive and positive reviews.

References

Abers, G. A., and R. McCaffrey (1994), Active arc-continent collision: Earthquakes, gravity anomalies, and fault kinematics in the Huon-Finisterre collision zone, Papua New Guinea, *Tectonics*, *13*(2), 227–245, doi:10.1029/93TC02940.

Adam, J., J. L. Urai, B. Wieneke, O. Oncken, K. Pfeiffer, N. Kukowski, J. Lohrmann, S. Hoth, W. Van Der Zee, and J. Schmatz (2005), Shear localisation and strain distribution during tectonic faulting—New insights from granular-flow experiments and high-resolution optical image correlation techniques, *J. Struct. Geol.*, *27*, 283–301, doi:10.1016/j.jsg.2004.08.008.

Afonso, J.-C., and S. Zlotnik (2011), The subductability of the continental lithosphere: The before and after story, in *Arc-Continent Collision*, edited by D. Brown and P. Ryan, pp. 53–86, Springer, Berlin, doi:10.1007/978-3-540-88558-0_3.

Anderson, D. L. (1995), Lithosphere, asthenosphere, and perisphere, *Rev. Geophys.*, *33*, 125–149, doi:10.1029/94RG02785.

Avé Lallemant, H., and L. R. Guth (1990), Role of extensional tectonics in exhumation of eclogites and blueschists in an oblique subduction setting: Northeastern Venezuela, *Geology*, *18*, 950–953, doi:10.1130/0091-7613(1990)018<0950:ROETIE>2.3.CO;2.

Beck, M. E. (1983), On the mechanism of tectonic transport in zones of oblique subduction, *Tectonophysics*, *93*, 1–11, doi:10.1016/0040-1951(83)90230-5.

Beck, M. E. (1991), Coastwise transport reconsidered: Lateral displacements in oblique subduction zones, and tectonic consequences, *Phys. Earth Planet. Inter.*, *68*, 1–8, doi:10.1016/0031-9201(91)90002-Y.

Beck, M. E., C. Rojas, and J. Cembrano (1993), On the nature of buttressing in margin-parallel strike-slip fault systems, *Geology*, *21*, 755–758, doi:10.1130/0091-7613(1993)021<0755:OTNOBI>2.3.CO;2.

Bellahsen, N., C. Faccenna, F. Funiciello, J. M. Daniel, and L. Jolivet (2003), Why did Arabia separate from Africa? Insights from 3-D laboratory experiments, *Earth Planet. Sci. Lett.*, *216*, 365–381, doi:10.1016/S0012-821X(03)00516-8.

Bellahsen, N., C. Faccenna, and F. Funiciello (2005), Dynamics of subduction and plate motion in laboratory experiments: Insights into the "plate tectonics" behavior of the Earth, *J. Geophys. Res.*, *110*, B01401, doi:10.1029/2004JB002999.

Bock, Y., L. Prawirodirdjo, J. F. Genrich, C. W. Stevens, R. McCaffrey, C. Subarya, S. S. O. Puntodewo, and E. Calais (2003), Crustal motion in Indonesia from Global Positioning System measurements, *J. Geophys. Res.*, *108*(B8), 2367, doi:10.1029/2001JB000324.

Boutelier, D., and A. Chemenda (2008), Exhumation of UHP/LT rocks due to the local reduction of the interplate pressure: Thermo-mechanical physical modelling, *Earth Planet. Sci. Lett.*, *271*, 226–232, doi:10.1016/j.epsl.2008.04.011.

Boutelier, D., and A. Chemenda (2011), Physical modeling of arc-continent collision: A review of 2-D, 3-D, purely mechanical and thermo-mechanical experimental models, in *Arc-Continent Collision*, edited by D. Brown and P. Ryan, pp. 445–473, Springer, Berlin, doi:10.1007/978-3-540-88558-0_16.

Boutelier, D. A., and O. Oncken (2010), Role of the plate margin curvature in the plateau buildup: Consequences for the central Andes, *J. Geophys. Res.*, *115*, B04402, doi:10.1029/2009JB006296.

Boutelier, D., and O. Oncken (2011), 3-D thermo-mechanical laboratory modeling of plate-tectonics: Modeling scheme, technique and first experiments, *Solid Earth*, *2*, 35–51, doi:10.5194/se-2-35-2011.

Boutelier, D., A. Chemenda, and C. Jorand (2002), Thermo-mechanical laboratory modelling of continental subduction: First experiments, *J. Virtual Explorer*, *6*, 61–65.

Boutelier, D., A. Chemenda, and J.-P. Burg (2003), Subduction versus accretion of intra-oceanic volcanic arcs: Insight from thermo-mechanical analog experiments, *Earth Planet. Sci. Lett.*, *212*, 31–45, doi:10.1016/S0012-821X(03)00239-5.

Boutelier, D., A. Chemenda, and C. Jorand (2004), Continental subduction and exhumation of high-pressure rocks: Insights from thermo-mechanical laboratory modelling, *Earth Planet. Sci. Lett.*, *222*, 209–216, doi:10.1016/j.epsl.2004.02.013.

Buckingham, E. (1914), On physically similar systems; illustrations of the use of dimensional equations, *Phys. Rev.*, *4*, 345–376, doi:10.1103/PhysRev.4.345.

Chemenda, A., M. Mattauer, J. Malavieille, and A. N. Bokun (1995), A mechanism for syn-collisional rock exhumation and associated normal faulting: Results from physical modelling, *Earth Planet. Sci. Lett.*, *132*, 225–232, doi:10.1016/0012-821X(95)00042-B.

Chemenda, A., M. Mattauer, and A. Bokun (1996), Continental subduction and a mechanism for exhumation of high-pressure metamorphic rocks: New modelling and field data from Oman, *Earth Planet. Sci. Lett.*, *143*, 173–182, doi:10.1016/0012-821X(96)00123-9.

Chemenda, A., P. Matte, and V. Sokolov (1997), A model of Palaeozoic obduction and exhumation of high-pressure/low-temperature rocks in the southern Urals, *Tectonophysics*, *276*, 217–227, doi:10.1016/S0040-1951(97)00057-7.

Chemenda, A., J.-P. Burg, and M. Mattauer (2000a), Evolutionary model of the Himalaya–Tibet system: Geopoem based on new modelling, geological and geophysical data, *Earth Planet. Sci. Lett.*, *174*, 397–409, doi:10.1016/S0012-821X(99)00277-0.

Chemenda, A., S. Lallemand, and A. Bokun (2000b), Strain partitioning and interplate friction in oblique subduction zones: Constraints provided by experimental modeling, *J. Geophys. Res.*, *105*, 5567–5581, doi:10.1029/1999JB900332.

Chemenda, A., D. Hurpin, J.-C. Tang, J.-F. Stephan, and G. Buffet (2001), Impact of arc-continent collision on the conditions of burial and exhumation of UHP/LT rocks: Experimental and numerical modelling, *Tectonophysics*, *342*, 137–161, doi:10.1016/S0040-1951(01)00160-3.

Currie, C. A., K. Wang, R. D. Hyndman, and J. He (2004), The thermal effects of steady-state slab-driven mantle flow above a subducting plate: The Cascadia subduction zone and backarc, *Earth Planet. Sci. Lett.*, *223*, 35–48, doi:10.1016/j.epsl.2004.04.020.

Currie, C. A., R. S. Huismans, and C. Beaumont (2008), Thinning of continental backarc lithosphere by flow-induced gravitational instability, *Earth Planet. Sci. Lett.*, *269*, 436–447, doi:10.1016/j.epsl.2008.02.037.

Davis, D., J. Suppe, and F. Dahlen (1983), Mechanics of fold-and-thrust belts and accretionary wedges, *J. Geophys. Res.*, *88*, 1153–1172, doi:10.1029/JB088iB02p01153.

Davy, P., and P. R. Cobbold (1991), Experiments on shortening of a 4-layer model of the continental lithosphere, *Tectonophysics*, *188*, 1–25, doi:10.1016/0040-1951(91)90311-F.

Dymkova, D., T. Gerya, S. W. Faryad, and J.-P. Burg (2010), Arc-continent collision: Insight from self-consistent numerical modeling, *Geophys. Res. Abstr.*, *12*, 2765.

Fitch, T. (1972), Plate convergence, transcurrent faults, and internal deformation adjacent to southeast Asia and the western Pacific, *J. Geophys. Res.*, *77*, 4432–4460, doi:10.1029/JB077i023p04432.

Funiciello, F., C. Faccenna, and D. Giardini (2004), Role of lateral mantle flow in the evolution of subduction systems: Insights from laboratory experiments, *Geophys. J. Int.*, *157*, 1393–1406, doi:10.1111/j.1365-246X.2004.02313.x.

Furukawa, Y. (1993), Magmatic processes under arcs and formation of the volcanic front, *J. Geophys. Res.*, *98*, 8309–8319, doi:10.1029/93JB00350.

Genrich, J. F., Y. Bock, R. McCaffrey, E. Calais, C. W. Stevens, and C. Subarya (1996), Accretion of the southern Banda arc to the Australian plate margin determined by Global Positioning System measurements, *Tectonics*, *15*, 288–295, doi:10.1029/95TC03850.

Harris, R. (2011), The nature of the Banda arc-continent collision in the Timor region, in *Arc-Continent Collision*, edited by D. Brown and P. Ryan, pp. 163–211, Springer, Berlin, doi:10.1007/978-3-540-88558-0_7.

Hoth, S., J. Adam, N. Kukowski, and O. Oncken (2006), Influence of erosion on the kinematics of bivergent orogens: Results from scaled sandbox simulations, in *Tectonics, Climate, and Landscape Evolution*, edited by S. D. Willett et al., *Spec. Pap. Geol. Soc. Am.*, *398*, 201–225, doi:10.1130/2006.2398(12).

Hubbert, M. K. (1937), Theory of scale models as applied to the study of geologic structures, *Geol. Soc. Am. Bull.*, *48*, 1459–1519.

Huchon, P., and X. Le Pichon (1984), Sunda strait and central Sumatra fault, *Geology*, *12*, 668–672, doi:10.1130/0091-7613(1984)12<668:SSACSF>2.0.CO;2.

Jansma, P. E., and G. S. Mattioli (2005), GPS results from Puerto Rico and the Virgin Islands: Constraints on tectonic setting and rates of active faulting, *Spec. Pap. Geol. Soc. Am.*, *385*, 13–30.

Jarrard, R. (1986), Terrane motion by strike-slip faulting of forearc slivers, *Geology*, *14*, 780–783, doi:10.1130/0091-7613(1986)14<780:TMBSFO>2.0.CO;2.

Kaus, B. J. P., C. Steedman, and T. W. Becker (2008), From passive continental margin to mountain belt: Insights from analytical and numerical models and application to Taiwan, *Phys. Earth Planet. Inter.*, *171*, 235–251, doi:10.1016/j.pepi.2008.06.015.

Kelemen, P. B., J. L. Rilling, E. M. Parmentier, L. Mehl, and B. R. Hacker (2003), Thermal structure due to solid-state flow in the mantle wedge beneath arcs, in *Inside the Subduction Factory*, *Geophys. Monogr. Ser.*, vol. 138, pp. 293–311, AGU, Washington, D. C.

Malavieille, J., et al. (2002), Arc-continent collision in Taiwan: New marine observations and tectonic evolution, in *Geology and Geophysics of an Arc-Continent Collision, Taiwan*, edited by T. Byrne and C.-S. Liu, *Geol. Soc. Am. Spec.Pap.*, *358*, 187–211, doi:10.1130/0-8137-2358-2.187.

Malod, J. A., K. Karta, M. O. Beslier, and M. T. Zen (1995), From normal to oblique subduction: Tectonic relationships between Java and Sumatra, *J. Southeast Asian Earth Sci.*, *12*(1–2), 85–93, doi:10.1016/0743-9547(95)00023-2.

Moberly, R., G. L. Shepherd, and W. T. Coulbourn (1982), Forearc and other basins, continental margin of northern and southern Peru and adjacent Ecuador and Chile, *Geol. Soc. Spec. Publ.*, *10*, 171–189, doi:10.1144/GSL.SP.1982.010.01.11.

Nakamura, M. (2004), Crustal deformation in the central and southern Ryukyu Arc estimated from GPS data, *Earth Planet. Sci. Lett.*, *217*(3–4), 389–398, doi:10.1016/S0012-821X(03)00604-6.

Nugroho, H., R. Harris, A. W. Lestariya, and B. Maruf (2009), Plate boundary reorganization in the active Banda Arc-continent collision: Insights from new GPS measurements, *Tectonophysics*, *479*, 52–65, doi:10.1016/j.tecto.2009.01.026.

Peacock, S. M. (2003), Thermal structure and metamorphic evolution of subducting slabs, in *Inside the Subduction Factory*, *Geophys. Monogr. Ser.*,vol. 138, pp. 7–22, AGU, Washington, D. C.

Ramberg, H. (1967), *Gravity, Deformation and the Earth's Crust: As Studied by Centrifuged Models*, Academic, London.

Reston, T., and G. Manatschal (2011), Rifted margins: Building blocks of later collision, in *Arc-Continent Collision*, edited by D. Brown and P. Ryan, pp. 3–21, Springer, Berlin, doi:10.1007/978-3-540-88558-0_1.

Riller, U., D. Boutelier, C. Schrank, and A. R. Cruden (2010), Role of kilometer-scale weak circular heterogeneities on upper crustal deformation patterns: Evidence from scaled analog modeling and the Sudbury Basin, Canada, *Earth Planet. Sci. Lett.*, *297*, 587–597, doi:10.1016/j.epsl.2010.07.009.

Schellart, W. P. (2004), Kinematics of subduction and subduction-induced flow in the upper mantle, *J. Geophys. Res.*, *109*, B07401, doi:10.1029/2004JB002970.

Schmidt, M. W., and S. Poli (1998), Experimentally based water budgets for dehydrating slabs and consequences for arc magma generation, *Earth Planet. Sci. Lett.*, *163*, 361–379, doi:10.1016/S0012-821X(98)00142-3.

Schrank, C. E., D. A. Boutelier, and A. R. Cruden (2008), The analog shear zone: From rheology to associated geometry, *J. Struct. Geol.*, *30*, 177–193, doi:10.1016/j.jsg.2007.11.002.

Schreurs, G., et al. (2006), Analog benchmarks of shortening and extension experiments, in *Analog and Numerical Modelling of Crustal-Scale Processes*, *Geol. Soc. Spec. Publ.*, *253*, 1–27, doi:10.1144/GSL.SP.2006.253.01.01.

Shemenda, A. (1994), *Subduction: Insights From Physical Modeling*, 207 pp., Kluwer Acad, Dordrecht, Netherlands.

Siebert, L., and T. Simkin (2002), Volcanoes of the world: An illustrated catalog of Holocene volcanoes and their eruptions, Smithson. Inst. Global Volcanism Program Digital Inf. Ser., GVP-3, http://gcmd.nasa.gov/records/GCMD_GVP_Holocene_Volcanoes.html, Smithson. Inst., Washington, D. C.

Silver, E. A., D. Reed, R. McCaffrey, and Y. Joyodiwiryo (1983), Back arc thrusting in the eastern Sunda arc, Indonesia: A consequence of arc-continent collision, *J. Geophys. Res.*, *88*, 7429–7448, doi:10.1029/JB088iB09p07429.

Snyder, D., H. Prasetyo, D. Blundell, C. Pigram, A. Barber, A. Richardson, and S. Tjokosaproetro (1996), A dual doubly vergent orogen in the Banda arc continent-arc collision zone as observed on deep seismic reflection profiles, *Tectonics*, *15*, 34–53, doi:10.1029/95TC02352.

Suppe, J. (1984), Kinematics of arc-continent collision, flipping of subduction, and back-arc spreading near Taiwan, *Mem. Geol. Soc. China*, *6*, 21–33.

Susilohadi, S., C. Gaedicke, and Y. Djajadihardja (2009), Structures and sedimentary deposition in the Sunda Strait, Indonesia, *Tectonophysics*, *467*(1–4), 55–71, doi:10.1016/j.tecto.2008.12.015.

Tatsumi, Y., M. Sakuyama, H. Fukuyama, and I. Kushiro (1983), Generation of arc basalt magmas and thermal structure of the mantle wedge in subduction zones, *J. Geophys. Res.*, *88*, 5815–5825, doi:10.1029/JB088iB07p05815.

Turcotte, D. L., and G. Schubert (1982), *Geodynamics: Applications of Continuum Physics to Geological Problems*, John Wiley, New York.

Ulmer, P. (2001), Partial melting in the mantle wedge-the role of H_2O in the genesis of mantle-derived arc-related magmas, *Phys. Earth Planet. Inter.*, *127*, 215–232, doi:10.1016/S0031-9201(01)00229-1.

van Gestel, J.-P., P. Mann, J. F. Dolan, and N. R. Grindlay (1998), Structure and tectonics of the upper Cenozoic Puerto Rico-Virgin Islands carbonate platform as determined from seismic reflection studies, *J. Geophys. Res.*, *103*(B12), 30,505–30,530, doi:10.1029/98JB02341.

van Hunen, J., and M. Allen (2011), Continental collision and slab breakoff: A comparison of 3-D numerical models with observations, *Earth Planet. Sci. Lett.*, *302*, 27–37, doi:10.1016/j.epsl.2010.11.035.

Wallace, L. M., C. Stevens, E. Silver, R. McCaffrey, W. Loratung, S. Hasiata, R. Stanaway, R. Curley, R. Rosa, and J. Taugaloidi (2004), GPS and seismological constraints on active tectonics and arc-continent

collision in Papua New Guinea: Implications for mechanics of microplate rotations in a plate boundary zone, *J. Geophys. Res.*, *109*, B05404, doi:10.1029/2003JB002481.

Witt, C., and J. Bourgois (2009), Forearc basin formation in the tectonic wake of a collision-driven, coastwise migrating crustal block: The example of the North Andean block and the extensional Gulf of Guayaquil-Tumbes Basin (Ecuador-Peru border area), *Geol. Soc. Am. Bull.*, *122*(1–2), 89–108.

Witt, C., J. Bourgois, F. Michaud, M. Ordonez, N. Jimenez, and M. Sosson (2006), Development of the Gulf of Guayaquil (Ecuador) during the Quaternary as an effect of the North Andean block tectonic escape, *Tectonics*, *25*, TC3017, doi:10.1029/2004TC001723.

Yamato, P., F. Mouthereau, and E. Burov (2009), Taiwan mountain building: Insights from 2-D thermomechanical modelling of a rheologically stratified lithosphere, *Geophys. J. Int.*, *176*, 307–326, doi:10.1111/j.1365-246X.2008.03977.x.

Yu, S. B., H. Y. Chen, and L. C. Kuo (1997), Velocity field of GPS stations in the Taiwan area, *Tectonophysics*, *274*(1–3), 41–59, doi:10.1016/S0040-1951(96)00297-1.

Yu, S.-B., Y.-J. Hsu, T. Bacolcol, C.-C. Yang, Y.-C. Tsai, and R. Solidum (2012), Present-day crustal deformation along the Philippine Fault in Luzon, Philippines, *J. Asian Earth Sci.*, doi:10.1016/j.jseaes.2010.12.007, in press.

Zhao, D., A. Hasegawa, and H. Kanamori (1994), Deep structure of Japan subduction zone as derived from local, regional, and teleseismic events, *J. Geophys. Res.*, *99*, 22,313–22,329, doi:10.1029/94JB01149.

Zhao, D., Y. Xu, D. A. Wiens, L. R. Dorman, J. Hildebrand, and S. Webb (1997), Depth extent of the Lau back-arc spreading center and its relation to subduction processes, *Science*, *278*, 254–257, doi:10.1126/science.278.5336.254.

D. Boutelier and A. Cruden, School of Geosciences, Monash University, Clayton, Vic 3800, Australia. (david.boutelier@monash.edu)

O. Oncken, Helmholtz Centre Potsdam, GFZ German Research Centre for Geosciences, Telegrafenberg, D-14473 Potsdam, Germany.